

Version 2.0 as of March 9, 2011

Contact persons: Marc Besançon, Frédéric Déliot, Cécile Deterre

Alexander Grohsjean, Yvonne Peters, Elizaveta Shabalina, Slava Sharyy

To be submitted to PLB

Comment to d0-run2eb-010@fnal.gov

by XX FNAL time

DØ INTERNAL DOCUMENT – NOT FOR PUBLIC DISTRIBUTION

author list dated 17 February 2011

1 Measurement of the $t\bar{t}$ production cross section using dilepton events in $p\bar{p}$ collisions

2 V.M. Abazov,³⁵ B. Abbott,⁷³ B.S. Acharya,²⁹ M. Adams,⁴⁹ T. Adams,⁴⁷ G.D. Alexeev,³⁵ G. Alkhazov,³⁹
3 A. Alton^{a,61} G. Alverson,⁶⁰ G.A. Alves,² L.S. Ancu,³⁴ M. Aoki,⁴⁸ M. Arov,⁵⁸ A. Askew,⁴⁷ B. Åsman,⁴¹
4 O. Atramentov,⁶⁵ C. Avila,⁸ J. BackusMayes,⁸⁰ F. Badaud,¹³ L. Bagby,⁴⁸ B. Baldin,⁴⁸ D.V. Bandurin,⁴⁷
5 S. Banerjee,²⁹ E. Barberis,⁶⁰ P. Baringer,⁵⁶ J. Barreto,³ J.F. Bartlett,⁴⁸ U. Bassler,¹⁸ V. Bazterra,⁴⁹ S. Beale,⁶
6 A. Bean,⁵⁶ M. Begalli,³ M. Begel,⁷¹ C. Belanger-Champagne,⁴¹ L. Bellantoni,⁴⁸ S.B. Beri,²⁷ G. Bernardi,¹⁷
7 R. Bernhard,²² I. Bertram,⁴² M. Besançon,¹⁸ R. Beuselinck,⁴³ V.A. Bezzubov,³⁸ P.C. Bhat,⁴⁸ V. Bhatnagar,²⁷
8 G. Blazey,⁵⁰ S. Blessing,⁴⁷ K. Bloom,⁶⁴ A. Boehnlein,⁴⁸ D. Boline,⁷⁰ T.A. Bolton,⁵⁷ E.E. Boos,³⁷ G. Borissov,⁴²
9 T. Bose,⁵⁹ A. Brandt,⁷⁶ O. Brandt,²³ R. Brock,⁶² G. Brooijmans,⁶⁸ A. Bross,⁴⁸ D. Brown,¹⁷ J. Brown,¹⁷ X.B. Bu,⁴⁸
10 M. Buehler,⁷⁹ V. Buescher,²⁴ V. Bunichev,³⁷ S. Burdin^{b,42} T.H. Burnett,⁸⁰ C.P. Buszello,⁴¹ B. Calpas,¹⁵
11 E. Camacho-Pérez,³² M.A. Carrasco-Lizarraga,⁵⁶ B.C.K. Casey,⁴⁸ H. Castilla-Valdez,³² S. Chakrabarti,⁷⁰
12 D. Chakraborty,⁵⁰ K.M. Chan,⁵⁴ A. Chandra,⁷⁸ G. Chen,⁵⁶ S. Chevalier-Théry,¹⁸ D.K. Cho,⁷⁵ S.W. Cho,³¹
13 S. Choi,³¹ B. Choudhary,²⁸ T. Christoudias,⁴³ S. Cihangir,⁴⁸ D. Claes,⁶⁴ J. Clutter,⁵⁶ M. Cooke,⁴⁸ W.E. Cooper,⁴⁸
14 M. Corcoran,⁷⁸ F. Couderc,¹⁸ M.-C. Cousinou,¹⁵ A. Croc,¹⁸ D. Cutts,⁷⁵ A. Das,⁴⁵ G. Davies,⁴³ K. De,⁷⁶
15 S.J. de Jong,³⁴ E. De La Cruz-Burelo,³² F. Déliot,¹⁸ M. Demarteau,⁴⁸ R. Demina,⁶⁹ D. Denisov,⁴⁸ S.P. Denisov,³⁸
16 S. Desai,⁴⁸ K. DeVaughan,⁶⁴ H.T. Diehl,⁴⁸ M. Diesburg,⁴⁸ A. Dominguez,⁶⁴ T. Dorland,⁸⁰ A. Dubey,²⁸
17 L.V. Dudko,³⁷ D. Duggan,⁶⁵ A. Duperrin,¹⁵ S. Dutt,²⁷ A. Dyshkant,⁵⁰ M. Eads,⁶⁴ D. Edmunds,⁶² J. Ellison,⁴⁶
18 V.D. Elvira,⁴⁸ Y. Enari,¹⁷ H. Evans,⁵² A. Evdokimov,⁷¹ V.N. Evdokimov,³⁸ G. Facini,⁶⁰ T. Ferbel,⁶⁹ F. Fiedler,²⁴
19 F. Filthaut,³⁴ W. Fisher,⁶² H.E. Fisk,⁴⁸ M. Fortner,⁵⁰ H. Fox,⁴² S. Fuess,⁴⁸ T. Gadfort,⁷¹ A. Garcia-Bellido,⁶⁹
20 V. Gavrilov,³⁶ P. Gay,¹³ W. Geist,¹⁹ W. Geng,^{15,62} D. Gerbaudo,⁶⁶ C.E. Gerber,⁴⁹ Y. Gershtein,⁶⁵ G. Ginther,^{48,69}
21 G. Golovanov,³⁵ A. Goussiou,⁸⁰ P.D. Grannis,⁷⁰ S. Greder,¹⁹ H. Greenlee,⁴⁸ Z.D. Greenwood,⁵⁸ E.M. Gregores,⁴
22 G. Grenier,²⁰ Ph. Gris,¹³ J.-F. Grivaz,¹⁶ A. Grohsjean,¹⁸ S. Grünendahl,⁴⁸ M.W. Grünewald,³⁰ T. Guillemin,¹⁶
23 F. Guo,⁷⁰ G. Gutierrez,⁴⁸ P. Gutierrez,⁷³ A. Haas^{c,68} S. Hagopian,⁴⁷ J. Haley,⁶⁰ L. Han,⁷ K. Harder,⁴⁴ A. Harel,⁶⁹
24 J.M. Hauptman,⁵⁵ J. Hays,⁴³ T. Head,⁴⁴ T. Hebbeker,²¹ D. Hedin,⁵⁰ H. Hegab,⁷⁴ A.P. Heinson,⁴⁶ U. Heintz,⁷⁵
25 C. Hensel,²³ I. Heredia-De La Cruz,³² K. Herner,⁶¹ G. Hesketh^{d,44} M.D. Hildreth,⁵⁴ R. Hirosky,⁷⁹ T. Hoang,⁴⁷
26 J.D. Hobbs,⁷⁰ B. Hoeneisen,¹² M. Hohlfield,²⁴ Z. Hubacek,^{10,18} N. Huske,¹⁷ V. Hynek,¹⁰ I. Iashvili,⁶⁷
27 R. Illingworth,⁴⁸ A.S. Ito,⁴⁸ S. Jabeen,⁷⁵ M. Jaffré,¹⁶ D. Jamin,¹⁵ A. Jayasinghe,⁷³ R. Jesik,⁴³ K. Johns,⁴⁵
28 M. Johnson,⁴⁸ D. Johnston,⁶⁴ A. Jonckheere,⁴⁸ P. Jonsson,⁴³ J. Joshi,²⁷ A. Juste,⁴⁰ K. Kaadze,⁵⁷ E. Kajfasz,¹⁵
29 D. Karmanov,³⁷ P.A. Kasper,⁴⁸ I. Katsanos,⁶⁴ R. Kehoe,⁷⁷ S. Kermiche,¹⁵ N. Khalatyan,⁴⁸ A. Khanov,⁷⁴
30 A. Kharchilava,⁶⁷ Y.N. Khazheev,³⁵ D. Khatidze,⁷⁵ M.H. Kirby,⁵¹ J.M. Kohli,²⁷ A.V. Kozelov,³⁸ J. Kraus,⁶²
31 S. Kulikov,³⁸ A. Kumar,⁶⁷ A. Kupco,¹¹ T. Kurča,²⁰ V.A. Kuzmin,³⁷ J. Kvita,⁹ S. Lammers,⁵² G. Landsberg,⁷⁵
32 P. Lebrun,²⁰ H.S. Lee,³¹ S.W. Lee,⁵⁵ W.M. Lee,⁴⁸ J. Lellouch,¹⁷ L. Li,⁴⁶ Q.Z. Li,⁴⁸ S.M. Lietti,⁵ J.K. Lim,³¹
33 D. Lincoln,⁴⁸ J. Linnemann,⁶² V.V. Lipaev,³⁸ R. Lipton,⁴⁸ Y. Liu,⁷ Z. Liu,⁶ A. Lobodenko,³⁹ M. Lokajicek,¹¹
34 R. Lopes de Sa,⁷⁰ H.J. Lubatti,⁸⁰ R. Luna-Garcia^{e,32} A.L. Lyon,⁴⁸ A.K.A. Maciel,² D. Mackin,⁷⁸ R. Madar,¹⁸
35 R. Magaña-Villalba,³² S. Malik,⁶⁴ V.L. Malyshev,³⁵ Y. Maravin,⁵⁷ J. Martínez-Ortega,³² R. McCarthy,⁷⁰
36 C.L. McGivern,⁵⁶ M.M. Meijer,³⁴ A. Melnitchouk,⁶³ D. Menezes,⁵⁰ P.G. Mercadante,⁴ M. Merkin,³⁷ A. Meyer,²¹
37 J. Meyer,²³ F. Miconi,¹⁹ N.K. Mondal,²⁹ G.S. Muanza,¹⁵ M. Mulhearn,⁷⁹ E. Nagy,¹⁵ M. Naimuddin,²⁸ M. Narain,⁷⁵
38 R. Nayyar,²⁸ H.A. Neal,⁶¹ J.P. Negret,⁸ P. Neustroev,³⁹ S.F. Novaes,⁵ T. Nunnemann,²⁵ G. Obrant,³⁹ J. Orduna,⁷⁸
39 N. Osman,¹⁵ J. Osta,⁵⁴ G.J. Otero y Garzón,¹ M. Padilla,⁴⁶ A. Pal,⁷⁶ M. Pangilinan,⁷⁵ N. Parashar,⁵³
40 V. Parihar,⁷⁵ S.K. Park,³¹ J. Parsons,⁶⁸ R. Partridge^{c,75} N. Parua,⁵² A. Patwa,⁷¹ B. Penning,⁴⁸ M. Perfilov,³⁷
41 K. Peters,⁴⁴ Y. Peters,⁴⁴ K. Petridis,⁴⁴ G. Petrillo,⁶⁹ P. Pétrouff,¹⁶ R. Piegaia,¹ J. Piper,⁶² M.-A. Pleier,⁷¹
42 P.L.M. Podesta-Lerma^{f,32} V.M. Podstavkov,⁴⁸ M.-E. Pol,² P. Polozov,³⁶ A.V. Popov,³⁸ M. Prewitt,⁷⁸ D. Price,⁵²
43 N. Prokopenko,³⁸ S. Protopopescu,⁷¹ J. Qian,⁶¹ A. Quadt,²³ B. Quinn,⁶³ M.S. Rangel,² K. Ranjan,²⁸ P.N. Ratoff,⁴²
44 I. Razumov,³⁸ P. Renkel,⁷⁷ M. Rijssenbeek,⁷⁰ I. Ripp-Baudot,¹⁹ F. Rizatdinova,⁷⁴ M. Rominsky,⁴⁸ A. Ross,⁴²

45 C. Royon,¹⁸ P. Rubinov,⁴⁸ R. Ruchti,⁵⁴ G. Safronov,³⁶ G. Sajot,¹⁴ P. Salcido,⁵⁰ A. Sánchez-Hernández,³²
 46 M.P. Sanders,²⁵ B. Sanghi,⁴⁸ A.S. Santos,⁵ G. Savage,⁴⁸ L. Sawyer,⁵⁸ T. Scanlon,⁴³ R.D. Schamberger,⁷⁰
 47 Y. Scheglov,³⁹ H. Schellman,⁵¹ T. Schliephake,²⁶ S. Schlobohm,⁸⁰ C. Schwanenberger,⁴⁴ R. Schwienhorst,⁶²
 48 J. Sekaric,⁵⁶ H. Severini,⁷³ E. Shabalina,²³ V. Shary,¹⁸ A.A. Shchukin,³⁸ R.K. Shivpuri,²⁸ V. Simak,¹⁰
 49 V. Sirotenko,⁴⁸ P. Skubic,⁷³ P. Slattery,⁶⁹ D. Smirnov,⁵⁴ K.J. Smith,⁶⁷ G.R. Snow,⁶⁴ J. Snow,⁷² S. Snyder,⁷¹
 50 S. Söldner-Rembold,⁴⁴ L. Sonnenschein,²¹ K. Soustruznik,⁹ J. Stark,¹⁴ V. Stolin,³⁶ D.A. Stoyanova,³⁸ M. Strauss,⁷³
 51 D. Strom,⁴⁹ L. Stutte,⁴⁸ L. Suter,⁴⁴ P. Svoisky,⁷³ M. Takahashi,⁴⁴ A. Tanasijczuk,¹ W. Taylor,⁶ M. Titov,¹⁸
 52 V.V. Tokmenin,³⁵ Y.-T. Tsai,⁶⁹ D. Tsybychev,⁷⁰ B. Tuchming,¹⁸ C. Tully,⁶⁶ P.M. Tuts,⁶⁸ L. Uvarov,³⁹ S. Uvarov,³⁹
 53 S. Uzunyan,⁵⁰ R. Van Kooten,⁵² W.M. van Leeuwen,³³ N. Varelas,⁴⁹ E.W. Varnes,⁴⁵ I.A. Vasilyev,³⁸ P. Verdier,²⁰
 54 L.S. Vertogradov,³⁵ M. Verzocchi,⁴⁸ M. Vesterinen,⁴⁴ D. Vilanova,¹⁸ P. Vint,⁴³ P. Vokac,¹⁰ H.D. Wahl,⁴⁷
 55 M.H.L.S. Wang,⁶⁹ J. Warchol,⁵⁴ G. Watts,⁸⁰ M. Wayne,⁵⁴ M. Weber,^{9,48} L. Welty-Rieger,⁵¹ A. White,⁷⁶ D. Wicke,²⁶
 56 M.R.J. Williams,⁴² G.W. Wilson,⁵⁶ M. Wobisch,⁵⁸ D.R. Wood,⁶⁰ T.R. Wyatt,⁴⁴ Y. Xie,⁴⁸ C. Xu,⁶¹ S. Yacoob,⁵¹
 57 R. Yamada,⁴⁸ W.-C. Yang,⁴⁴ T. Yasuda,⁴⁸ Y.A. Yatsunenko,³⁵ Z. Ye,⁴⁸ H. Yin,⁴⁸ K. Yip,⁷¹ S.W. Youn,⁴⁸
 58 J. Yu,⁷⁶ S. Zelitch,⁷⁹ T. Zhao,⁸⁰ B. Zhou,⁶¹ J. Zhu,⁶¹ M. Zielinski,⁶⁹ D. Zieminska,⁵² and L. Zivkovic⁷⁵

(The D0 Collaboration*)

¹Universidad de Buenos Aires, Buenos Aires, Argentina

²LAFEX, Centro Brasileiro de Pesquisas Físicas, Rio de Janeiro, Brazil

³Universidade do Estado do Rio de Janeiro, Rio de Janeiro, Brazil

⁴Universidade Federal do ABC, Santo André, Brazil

⁵Instituto de Física Teórica, Universidade Estadual Paulista, São Paulo, Brazil

⁶Simon Fraser University, Vancouver, British Columbia, and York University, Toronto, Ontario, Canada

⁷University of Science and Technology of China, Hefei, People's Republic of China

⁸Universidad de los Andes, Bogotá, Colombia

⁹Charles University, Faculty of Mathematics and Physics,
Center for Particle Physics, Prague, Czech Republic

¹⁰Czech Technical University in Prague, Prague, Czech Republic

¹¹Center for Particle Physics, Institute of Physics,
Academy of Sciences of the Czech Republic, Prague, Czech Republic

¹²Universidad San Francisco de Quito, Quito, Ecuador

¹³LPC, Université Blaise Pascal, CNRS/IN2P3, Clermont, France

¹⁴LPSC, Université Joseph Fourier Grenoble 1, CNRS/IN2P3,

Institut National Polytechnique de Grenoble, Grenoble, France

¹⁵CPPM, Aix-Marseille Université, CNRS/IN2P3, Marseille, France

¹⁶LAL, Université Paris-Sud, CNRS/IN2P3, Orsay, France

¹⁷LPNHE, Universités Paris VI and VII, CNRS/IN2P3, Paris, France

¹⁸CEA, Irfu, SPP, Saclay, France

¹⁹IPHC, Université de Strasbourg, CNRS/IN2P3, Strasbourg, France

²⁰IPNL, Université Lyon 1, CNRS/IN2P3, Villeurbanne, France and Université de Lyon, Lyon, France

²¹III. Physikalisches Institut A, RWTH Aachen University, Aachen, Germany

²²Physikalisches Institut, Universität Freiburg, Freiburg, Germany

²³II. Physikalisches Institut, Georg-August-Universität Göttingen, Göttingen, Germany

²⁴Institut für Physik, Universität Mainz, Mainz, Germany

²⁵Ludwig-Maximilians-Universität München, München, Germany

²⁶Fachbereich Physik, Bergische Universität Wuppertal, Wuppertal, Germany

²⁷Panjab University, Chandigarh, India

²⁸Delhi University, Delhi, India

²⁹Tata Institute of Fundamental Research, Mumbai, India

³⁰University College Dublin, Dublin, Ireland

³¹Korea Detector Laboratory, Korea University, Seoul, Korea

³²CINVESTAV, Mexico City, Mexico

³³FOM-Institute NIKHEF and University of Amsterdam/NIKHEF, Amsterdam, The Netherlands

³⁴Radboud University Nijmegen/NIKHEF, Nijmegen, The Netherlands

³⁵Joint Institute for Nuclear Research, Dubna, Russia

³⁶Institute for Theoretical and Experimental Physics, Moscow, Russia

³⁷Moscow State University, Moscow, Russia

³⁸Institute for High Energy Physics, Protvino, Russia

³⁹Petersburg Nuclear Physics Institute, St. Petersburg, Russia

⁴⁰Institució Catalana de Recerca i Estudis Avançats (ICREA) and Institut de Física d'Altes Energies (IFAE), Barcelona, Spain

⁴¹Stockholm University, Stockholm and Uppsala University, Uppsala, Sweden

⁴²Lancaster University, Lancaster LA1 4YB, United Kingdom

- 105 ⁴³Imperial College London, London SW7 2AZ, United Kingdom
 106 ⁴⁴The University of Manchester, Manchester M13 9PL, United Kingdom
 107 ⁴⁵University of Arizona, Tucson, Arizona 85721, USA
 108 ⁴⁶University of California Riverside, Riverside, California 92521, USA
 109 ⁴⁷Florida State University, Tallahassee, Florida 32306, USA
 110 ⁴⁸Fermi National Accelerator Laboratory, Batavia, Illinois 60510, USA
 111 ⁴⁹University of Illinois at Chicago, Chicago, Illinois 60607, USA
 112 ⁵⁰Northern Illinois University, DeKalb, Illinois 60115, USA
 113 ⁵¹Northwestern University, Evanston, Illinois 60208, USA
 114 ⁵²Indiana University, Bloomington, Indiana 47405, USA
 115 ⁵³Purdue University Calumet, Hammond, Indiana 46323, USA
 116 ⁵⁴University of Notre Dame, Notre Dame, Indiana 46556, USA
 117 ⁵⁵Iowa State University, Ames, Iowa 50011, USA
 118 ⁵⁶University of Kansas, Lawrence, Kansas 66045, USA
 119 ⁵⁷Kansas State University, Manhattan, Kansas 66506, USA
 120 ⁵⁸Louisiana Tech University, Ruston, Louisiana 71272, USA
 121 ⁵⁹Boston University, Boston, Massachusetts 02215, USA
 122 ⁶⁰Northeastern University, Boston, Massachusetts 02115, USA
 123 ⁶¹University of Michigan, Ann Arbor, Michigan 48109, USA
 124 ⁶²Michigan State University, East Lansing, Michigan 48824, USA
 125 ⁶³University of Mississippi, University, Mississippi 38677, USA
 126 ⁶⁴University of Nebraska, Lincoln, Nebraska 68588, USA
 127 ⁶⁵Rutgers University, Piscataway, New Jersey 08855, USA
 128 ⁶⁶Princeton University, Princeton, New Jersey 08544, USA
 129 ⁶⁷State University of New York, Buffalo, New York 14260, USA
 130 ⁶⁸Columbia University, New York, New York 10027, USA
 131 ⁶⁹University of Rochester, Rochester, New York 14627, USA
 132 ⁷⁰State University of New York, Stony Brook, New York 11794, USA
 133 ⁷¹Brookhaven National Laboratory, Upton, New York 11973, USA
 134 ⁷²Langston University, Langston, Oklahoma 73050, USA
 135 ⁷³University of Oklahoma, Norman, Oklahoma 73019, USA
 136 ⁷⁴Oklahoma State University, Stillwater, Oklahoma 74078, USA
 137 ⁷⁵Brown University, Providence, Rhode Island 02912, USA
 138 ⁷⁶University of Texas, Arlington, Texas 76019, USA
 139 ⁷⁷Southern Methodist University, Dallas, Texas 75275, USA
 140 ⁷⁸Rice University, Houston, Texas 77005, USA
 141 ⁷⁹University of Virginia, Charlottesville, Virginia 22901, USA
 142 ⁸⁰University of Washington, Seattle, Washington 98195, USA

We present a measurement of the top quark-antiquark pair production cross section in $p\bar{p}$ collisions at $\sqrt{s} = 1.96$ TeV using 5.4 fb^{-1} of data collected with the D0 detector. We consider decay channels with two electrons, two muons or one electron and one muon in the final state. For a top quark mass of $m_t = 172.5$ GeV, the measured cross section is $7.4_{-0.8}^{+0.9}$ (stat + syst) pb. This result combined with the cross section measurement in the lepton + jets final state yields a cross section of 7.6 ± 0.6 (stat + syst) pb which agrees with the standard model expectation.

PACS numbers: 14.65.Ha, 13.85.Lg, 13.85.Qk, 14.60.Fg, 12.15.Ff

I. INTRODUCTION

Precisely measuring the top quark pair ($t\bar{t}$) production cross section ($\sigma_{t\bar{t}}$) and comparing such a measurement with the current most precise predictions from the standard model (SM) provides an important test of perturbative Quantum Chromodynamics (QCD). Currently the most precise predictions of $\sigma_{t\bar{t}}$ are given by approximate next to next to leading order (NNLO) calculations [1–3] with a precision of 6% to 9% which challenge the experimental precision for the measurement of $\sigma_{t\bar{t}}$. Measuring $\sigma_{t\bar{t}}$ can furthermore be used to measure the top quark mass (m_t) providing an additional knowledge of this SM parameter [4, 5]. Any significant deviation from

the SM prediction of $\sigma_{t\bar{t}}$ can be interpreted as a hint for the presence of physics beyond the SM. In absence of such a deviation the measurement of $\sigma_{t\bar{t}}$ can in turn be used to constrain extensions of the SM such as scenarios in which the top quark would decay into a charged Higgs boson and a b quark [5].

In this letter we present an updated measurement of $\sigma_{t\bar{t}}$ in $p\bar{p}$ collisions at $\sqrt{s} = 1.96$ TeV in the dilepton ($\ell\bar{\ell}$) channel in which the W boson from each top quark decays leptonically into $e\nu_e$, $\mu\nu_\mu$ or $\tau\nu_\tau$ and the τ lepton further decays into $e\nu_e\nu_\tau$ or $\mu\nu_\mu\nu_\tau$, thus giving rise to the ee , $\mu\mu$ or $e\mu$ final states. This measurement complements the $\sigma_{t\bar{t}}$ measurements in the lepton+jets (ℓj) channel in which one of the W bosons from the top quark decays

*with visitors from ^aAugustana College, Sioux Falls, SD, USA, ^bThe University of Liverpool, Liverpool, UK, ^cSLAC, Menlo Park, CA, USA, ^dUniversity College London, London, UK, ^eCentro de Investigación en Computación, IPN, Mexico City, Mexico

hadronically into a $q\bar{q}'$ pair and the other W boson decays leptonically [6, 7] as well as measurements in the all hadronic channel in which both W bosons decay hadronically [8].

The measurement is based on data collected with the D0 detector during Run II of the Fermilab Tevatron collider and correspond to an integrated luminosity of $5.4 \pm 0.3 \text{ fb}^{-1}$. The result of this analysis surpasses our previous measurement [9] which was done with five times less data. The CDF collaboration has performed a $\sigma_{t\bar{t}}$ measurement in the $\ell\ell$ channel using 2.8 fb^{-1} [10]. The ATLAS and CMS collaborations recently published their first $\sigma_{t\bar{t}}$ measurements in pp collisions at $\sqrt{s} = 7 \text{ TeV}$ [11, 12].

The D0 detector is described in detail in [13]. The region of the D0 detector closest to the interaction point contains a tracking system consisting of a silicon microstrip tracker (SMT) and a central fiber tracker (CFT) both located inside a superconducting solenoid magnet which generates a magnetic field of 1.9T. Hits in these two detectors are used to reconstruct tracks from charged particles in the pseudorapidity region $|\eta| < 3$ [28]. Surrounding the two tracking subdetectors are liquid argon-uranium calorimeters, segmented into electromagnetic and hadronic sections. The central section of the calorimeter (CC) covers pseudorapidities $|\eta| < 1.1$ and the two end calorimeters (EC) extend coverage to $|\eta| \approx 4.2$ with all three housed in separate cryostats. The muon system surrounds the calorimeter and consists of three layers of tracking detectors and scintillator trigger counters covering $|\eta| < 2$. A toroidal iron magnet with a field of 1.8T is located outside the innermost layer of the muon detector. The luminosity is calculated from the rate of inelastic $p\bar{p}$ collisions measured with plastic scintillator arrays, located in front of the EC cryostats [14].

The D0 trigger is based on a three-level pipeline system. The first level is implemented in custom-designed hardware. The second level uses high-level processors to combine information from the different sub-detectors to construct simple physics objects. The software-based third level uses full event information obtained with a simplified reconstruction algorithm.

II. OBJECT IDENTIFICATION

The $t\bar{t}$ dilepton final state contain two leptons (electrons or muons), at least two jets and significant transverse missing momentum.

Electrons are identified as energy clusters with radius $R = \sqrt{\Delta\eta^2 + \Delta\phi^2} < 0.2$ in the calorimeter consistent in its profile with an electromagnetic shower. More than 90% of the energy of the electron candidate should be deposited in the electromagnetic part of the calorimeter and it should have less than 20% of its energy in a calorimeter annulus of $0.2 < R < 0.4$ around its direction. This cluster has to be matched to a track. We consider electrons in CC with $|\eta| < 1.1$ and in EC with $1.5 < |\eta| < 2.5$.

Additionally, we require an electron likelihood discriminant based on tracking and calorimeter information to be larger than 0.85.

A muon is identified as a segment in at least one layer of the outer muon chambers in the full acceptance of the D0 muon system, matched to a track in the central tracking system. Reconstructed muons should satisfy two isolation criteria. First, the transverse energy deposit in a calorimeter annulus around the muon $0.1 < R < 0.4$ ($E_T^{\mu \text{ iso}}$) has to be smaller than 15% of the transverse momentum of the muon (p_T^μ). Second, the sum of the p_T of the tracks in a cone of radius $R < 0.5$ around the muon track in the central tracking system ($p_T^{\mu \text{ iso}}$) has to be smaller than 15% of p_T^μ . Muons that fulfill these isolation criteria are referred to as tight isolated muons.

For events simulated with Monte Carlo (MC) the residual differences with data in the electron or muon p_T resolution and in the electron or muon identification efficiencies are corrected. These corrections are derived by measuring the efficiencies and resolutions in $Z/\gamma^* \rightarrow \ell\ell$ data and MC events, identifying one tight lepton as tag and using the other charged lepton as a probe (tag-and-probe method).

Jets are identified with a fixed cone algorithm with radius $R < 0.5$ [15]. We consider jets in the range $|\eta| < 2.5$. A jet energy scale correction (JES) is determined by calibrating the energy deposited in the jet cone using transverse momentum balance in γ +jet and dijet events. This correction also takes into account the presence of the muon in the jet cone. We require that the jets are matched to at least two tracks originating from the vertex of the primary interaction (PV). Jets in MC are corrected for the residual difference between data and MC in the energy resolution and JES. These correction factors are measured by comparing data and MC in $(Z/\gamma^* \rightarrow ee)$ +jets events.

We use a neural-network (NN) tagging algorithm [16] to identify jets from b quarks. The algorithm combines information from the impact parameter of the tracks and variables that characterize the presence and properties of secondary vertices within the jet. In order to use this information for b -tagging, the jet is required to be matched to a jet built from tracks. Jets fulfilling this requirement are called taggable jets.

Missing transverse momentum (\cancel{p}_T) is reconstructed from the energy deposited in the calorimeter cells. Correction for lepton and jet p_T 's are propagated into the \cancel{p}_T . Missing transverse momentum significance ($\sigma_{\cancel{p}_T}$) is defined in each event as \cancel{p}_T divided by its uncertainty.

More details about object identification can be found in [17].

III. EVENT SELECTION AND BACKGROUND ESTIMATION

The main sources of background in the $\ell\ell$ channel come from Drell-Yan and Z boson production ($Z/\gamma^* \rightarrow \ell\ell$),

diboson production (WW, WZ, ZZ) and instrumental background. The instrumental background mainly arises from multijet and W +jets events in which one or two jets are misidentified as electrons or an isolated muon originating of semileptonic decays of a heavy flavor quark emitted by jet.

For this analysis we consider events that fired a set of single lepton triggers for the ee and $\mu\mu$ channels. For the $e\mu$ channel we consider events selected by any trigger. Efficiencies for single lepton triggers have been measured using the tag-and-probe method with $Z/\gamma^* \rightarrow \ell\ell$ data. These efficiencies are found to be around 99% for the ee channel and 80% for the $\mu\mu$ final state. For the $e\mu$ channel the overall efficiency of single lepton and electron muon triggers are close to 100%.

In order to separate the $t\bar{t}$ signal events from background, the following selection is applied:

- We require at least one PV in the beam interaction region with $|Z| < 60$ cm, where Z is the coordinate along the beam axis and $Z=0$ in the center of the detector. At least three tracks must be associated with this PV.
- We require at least two isolated leptons with transverse momentum $p_T > 15$ GeV. These two leptons must originate from the same PV, i.e. the difference between the Z coordinates of the two lepton tracks should be less than 2 cm, where Z coordinate is calculated at the point of the track closest approach to the beam.
- We require the two selected leptons to have opposite site charge. For the instrumental background termination we also use events where both leptons have the same charge. We will refer to these events as the same sign sample. In the $e\mu$ final state we require the distance between the electron and the muon directions: $R(e, \mu) > 0.3$ to reduce the background from bremsstrahlung.
- We require at least two jets with $p_T > 20$ GeV. In the $e\mu$ channel, we also consider events with only one jet.
- To further improve the signal purity of the selected sample, we apply additional topological selections. In the $e\mu$ final state with two jets we require $H_T > 110$ GeV, where H_T is the scalar sum of the p_T 's of the two leading jets and the leading lepton. In the $e\mu$ channel with exactly one jet we require $H_T > 105$ GeV. In the ee final state, we require $\sigma_{\cancel{p}_T} > 5$ while in the $\mu\mu$ channel we require that $\cancel{p}_T > 40$ GeV and $\sigma_{\cancel{p}_T} > 5$.

In order to estimate the signal efficiency and the background contamination we use the MC simulation for all contributions but the instrumental background, the latter being derived with data. The $t\bar{t}$ and Z/γ^* events are generated with the tree level matrix element generator

ALPGEN [18] interfaced with the PYTHIA [19] generator for parton showering and hadronization. Diboson events are generated with PYTHIA. All simulated samples are generated using the CTEQ6L1 parton distribution functions (PDFs) [20]. The Z/γ^* samples are normalized to the NNLO cross section computed for different dilepton invariant mass ranges with the FEWZ program [21]. We simulate separately Z/γ^* with heavy flavor (HF) quarks $Z/\gamma^* + bb$ (or $Z/\gamma^* + cc$) using ALPGEN and enhance the corresponding leading order cross sections by a factor of 1.5 (1.7) estimated with the MCFM program [22]. The diboson samples are normalized to the next to leading order cross section calculated with MCFM. Uncertainties in these normalization factors are taken into account as systematic uncertainties. We additionally apply a correction to the $Z/\gamma^* + \text{jets}$ simulation to address the imperfect modeling of the Z boson p_T in the MC.

The instrumental background is estimated directly from data. First, in the ee and $e\mu$ channels we determine the contribution of events with jets misidentified as electrons using the signal data sample but without electron likelihood discriminant cut. We extract the number of events with misidentified jets, n_f , and the number of events with real electrons, n_e , by fitting the electron likelihood distribution with an extended likelihood fit, using the following likelihood function:

$$\mathcal{L} = \prod_{i=1}^N [n_e S(x_i) + n_f B(x_i)] \frac{e^{-n_e + n_f}}{N!}, \quad (1)$$

where N is the number of selected events and $S(x_i)$ and $B(x_i)$ are the signal and background probability density functions (pdf), and i runs over all selected events. The signal pdf is measured in $Z/\gamma^* \rightarrow ee$ data events. The background pdf is measured in the $e\mu$ same sign sample without any topological requirement but with muon anti-isolation cuts: $E_T^{\mu \text{ iso}}/p_T^\mu > 0.2$ and $p_T^{\mu \text{ iso}}/p_T^\mu > 0.2$. The total number of events with a jet misidentified as an electron in the signal selection can be found as $n = n_f \int_{0.85}^{1.0} B(x) dx$, where the integration is done over the high likelihood region. The estimation is performed separately in CC and EC. It was found that the contribution of instrumental background to the ee channel is negligible.

In a second step, we determine the number of events with an isolated muon arising from jets in the $e\mu$ and $\mu\mu$ channels. This number is estimated as $n_f^\mu = N_{\text{loose}} f_\mu$, where N_{loose} is the number of events in the same sign sample with loose isolation criteria on the muon: $E_T^{\mu \text{ iso}}/p_T^\mu < 0.5$ and $p_T^{\mu \text{ iso}}/p_T^\mu < 0.5$. In the $\mu\mu$ final state we apply these loose isolation cuts only to one randomly chosen muon. In the $e\mu$ channel, the number of events with jets misidentified as electrons in the same sign sample is subtracted from N_{loose} . The muon fake isolation rate f_μ is determined in a dimuon sample with at least one jet. In this sample we require one muon to be close to the jet ($dR(\mu, \text{jet}) < 0.5$) with anti-isolation cuts $E_T^{\mu \text{ iso}}/p_T^\mu > 0.15$ and $p_T^{\mu \text{ iso}}/p_T^\mu > 0.15$. The other muon

defined as the probe should pass the loose isolation cuts $E_T^{\mu iso}/p_T^\mu < 0.5$ and $p_T^{\mu iso}/p_T^\mu < 0.5$. We compute f_μ as the ratio of the number of events in which the probe muon passes the tight isolation cuts to the total number of events in this same-sign sample.

The number of predicted background events as well as the expected number of signal events in the different channels are shown in Table I. In order to achieve a better separation between signal and background when measuring the cross section we use the distribution of the smallest of the two b -tagging NN discriminant outputs of the two leading jets. These NN discriminant distributions for the different channels are shown in Fig. 1. We measure the $t\bar{t}$ cross section $\sigma_{t\bar{t}}$ by simultaneously fitting the NN distributions in the four channels and maximizing the following likelihood function:

$$\mathcal{L} = \prod_{i=1}^{i \leq 4} \prod_{j=1}^{j \leq 14} P(n_{ij}, \mu_{ij}(\sigma_{t\bar{t}})), \quad (2)$$

where i runs over the channels and j over the bins of the NN distribution, $P(n, \mu(\sigma_{t\bar{t}}))$ is the Poisson probability function to observe n events when $\mu(\sigma_{t\bar{t}})$ events are expected.

IV. RESULTS AND UNCERTAINTIES

Using the fit procedure described above we measure the $t\bar{t}$ cross section for a top quark mass of $m_t = 172.5$ GeV and we find:

$$\sigma_{t\bar{t}} = 8.0 \pm 0.5 (stat) \pm 1.0 (syst) \text{ pb}. \quad (3)$$

The main systematic uncertainties for this measurement are described in the following. The uncertainty in the measured integrated luminosity of 6.1% [14] affects directly the cross section measurement, but also the expected number of Z/γ^* and diboson background events. Uncertainties in lepton identification efficiencies are determined by evaluating the different sources of bias in the tag-and-probe method and data/MC differences in $Z/\gamma^* \rightarrow \ell\ell$ events. Uncertainties in the lepton energy resolution are determined by comparing the width of the Z boson invariant mass distribution in data and MC.

The uncertainty in the relative JES between data and MC for light quark jets is measured in $Z/\gamma^* + \text{jets}$ events. The uncertainty on the difference between light and b quark JES (1.8%) is estimated by propagating the difference in the single pion response between data and MC to the MC JES for b quark jets. Jet energy resolution uncertainties are estimated by comparing the resolution measured in $Z/\gamma^* + \text{jets}$ events in data and MC. The uncertainty on the jet identification efficiency is estimated by comparing the efficiency measured in dijet events data and MC. The b quark identification uncertainties include uncertainties in the probability to tag a b quark jet, the probability to tag a light quark jet and the probability for a jet not to be taggable [16].

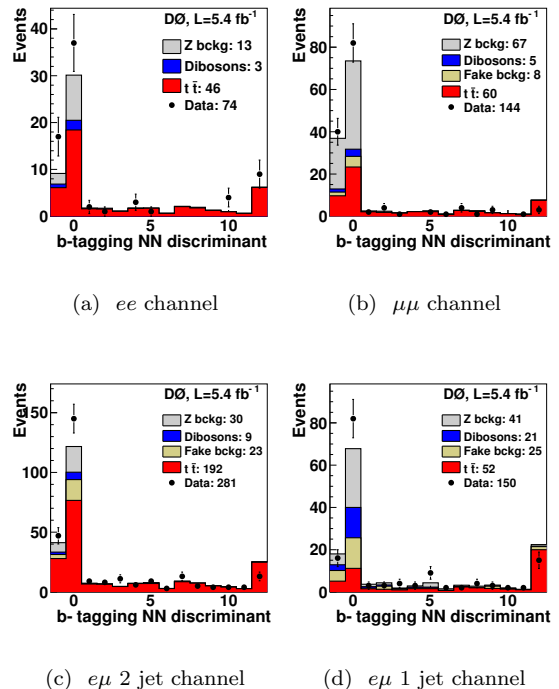


FIG. 1: Expected and observed distributions for the smallest b -tagging NN discriminant outputs of the two leading jets. The $t\bar{t}$ signal is normalized to the SM cross section (7.45 pb). The X axis represents the NN output non-uniformly mapped to 14 bins. The bin with central value 0 represents the lowest probability for a jet to be produced by a b quark. The bin with value 12 represents the highest probability. The bin with value -1 represents the jets which do not satisfy the requirements to enter to the NN computation (non-taggable jets).

To estimate the uncertainty in the trigger efficiency we use events selected with the same criteria as the $t\bar{t}$ signal but without any jet requirement. In all the channels this selection is dominated by Z/γ^* events. We compute the ratio of the expected and observed number of events for two cases: when both leptons are allowed to fire the trigger or when only one lepton is allowed to fire the trigger. The difference in these ratios is used to estimate the uncertainty on the trigger efficiency.

The systematic uncertainty due to the signal modeling comes from several effects. The effects of higher order corrections and hadronization modeling have been estimated as the difference in signal efficiency using the default ALPGEN+ PYTHIA simulation and using events generated with the MC@NLO [23] generator. The uncertainty coming from color reconnection is evaluated by comparing the $t\bar{t}$ efficiency using PYTHIA v6.4 tune Apr0 and PYTHIA v6.4 tune ACRpro [24]. The uncertainty on initial (ISR) and final (FSR) state radiation is evaluated by comparing the signal efficiency using PYTHIA with varied ISR/FSR parameters. The uncertainty due to PDF is estimated by reweighting the signal efficiency to CTEQ6.1M [25] and looking at the efficiency variation

TABLE I: Numbers of expected and observed events assuming the SM $t\bar{t}$ cross section for a top mass of $m_t = 172.5$ GeV (7.45 pb). The expected number of events is shown with its systematic uncertainties. The uncertainty on the ratio between observed and expected number of events takes into account the statistical uncertainty in the observed number of events and the systematic uncertainty in the expected number of events.

Channel	$Z \rightarrow \ell\ell$	Diboson	Instrumental background	$t\bar{t} \rightarrow \ell\bar{\ell}b\bar{b}\nu\bar{\nu}$	Expected N of events	Observed N of events	$\frac{Observed}{Expected}$
$e\mu$ two jets	30.3 ± 4.2	8.6 ± 1.2	22.7 ± 8.6	191.5 ± 18.8	253.1 ± 24.3	281	1.11 ± 0.13
$e\mu$ one jet	40.9 ± 4.8	20.7 ± 2.4	25.3 ± 10.5	52.1 ± 9.4	139.0 ± 16.5	150	1.08 ± 0.16
ee	12.6 ± 2.0	3.0 ± 0.4	-	45.6 ± 5.3	61.1 ± 7.1	74	1.21 ± 0.20
$\mu\mu$	67.3 ± 9.7	5.1 ± 0.7	7.6 ± 1.2	59.8 ± 6.6	139.8 ± 15.7	144	1.03 ± 0.14

along the 20 CTEQ6.1M eigenvector errors. The uncertainty due to the simulation of b quark fragmentation is assigned as the difference between tuning the parameters of the b quark fragmentation function to LEP or SLD data [26].

The uncertainty in the background normalization includes the theoretical uncertainties in the cross section and the uncertainty due to the correction for the Z boson p_T modeling. We also take into account an uncertainty due to the limited statistics of the signal and background templates of the NN discriminant. For the following systematic uncertainties we take into account the shapes changing effects of the b -tagging NN output discriminant: jet energy scale, jet resolution, jet identification and b quark identification uncertainties.

In order to reduce the influence of systematic uncertainties on the cross section measurement we use the nuisance parameters technique [27] to constrain the overall uncertainty using the data NN output distribution itself. Using this technique the likelihood (2) has to be modified to be:

$$\mathcal{L} = \prod_{i=1}^{i \leq 4} \prod_{j=1}^{j \leq 14} P(n_{ij}, \mu_{ij}(\sigma_{t\bar{t}})) \prod_k \mathcal{G}(\nu_k; 0, SD), \quad (4)$$

where k is an index running over all independent sources of systematic uncertainties. Each nuisance parameter ν_k is constrained by a Gaussian probability \mathcal{G} with mean at zero and width corresponding to one standard deviation (SD) for the considered systematic uncertainty. Correlations of systematic uncertainties between channels and between the different samples are naturally taken into account by assigning the same nuisance parameter to the correlated systematic uncertainty. In formula (4), the free parameters of the fit are ν_k and $\sigma_{t\bar{t}}$.

As can be seen from (3), the systematic uncertainties are the limiting uncertainties in the precision of the $t\bar{t}$ cross section measurement. Varying the systematic uncertainties and constraining them with data using the nuisance parameter technique can therefore significantly improve the measurement. Using the nuisance parameter technique we find an improved overall uncertainty of approximately 20% and reach a relative precision of 11% on the $t\bar{t}$ cross section:

$$\sigma_{t\bar{t}} = 7.4_{-0.8}^{+0.9} (\text{stat} + \text{syst}) \text{ pb}$$

for $m_t = 172.5$ GeV. The uncertainties in this measurement are summarized in Table II. For each category of systematic uncertainties listed in Table II, only the corresponding nuisance parameters are allowed to vary. The absolute shift of the measured $t\bar{t}$ cross section with respect to the result obtained including only statistical uncertainties is shown in the column “Offset”. In the columns “ $+\sigma$ ” and “ $-\sigma$ ” the systematic uncertainty on the measured cross section for each category are listed. The line “Fit result” contains the result of the full nuisance parameter fit, where all nuisance parameters are allowed to vary at the same time, which can result in a different “offset” and different uncertainties on the final $t\bar{t}$ cross section than expected from the sum of the individual “offsets” and systematic uncertainties. The uncertainty quoted in this line includes the full statistical and systematic uncertainty on the result.

Furthermore, we combine this measurement with the cross section measurement in the fully orthogonal ℓj channel [6] using the same nuisance parameter approach and taking all correlations into account. In the ℓj channel the events are separated into events with three or at least four jets, of which zero, one or at least two jets are b -tagged. For events with zero b -tags and three or at least four jets and events with one b -tagged jet and three jets a topological discriminant is used additionally. In Ref. [6] the separation into these channels and application of topological methods is referred to as the combined method. For this combination, we did not simultaneously fit the heavy flavor fraction for W +jet processes (W +HF) in the ℓj channel as was done in Ref. [6], making it unnecessary to use ℓj events with only two jets. With this change compared to Ref. [6] the measured ℓj $t\bar{t}$ cross section for $m_t = 172.5$ GeV is:

$$\sigma_{t\bar{t}} = 7.9_{-0.7}^{+0.8} (\text{stat} + \text{syst}) \text{ pb.}$$

The combination of the measurements in the ℓj and $\ell\ell$ final states is done by maximizing the product of the likelihood function for dilepton (4) and the likelihood function of the ℓj channel [6], which yields:

$$\sigma_{t\bar{t}} = 7.6 \pm 0.6 (\text{stat} + \text{syst}) \text{ pb}$$

for $m_t = 172.5$ GeV. This combination has a relative precision of 8% and represents an improvement of about 12% relative to the ℓj cross section measurement alone. The

TABLE II: Measured $t\bar{t}$ cross section with the breakdown of uncertainties in the $\ell\ell$ channel and for the combined $\ell\ell$ and ℓj measurement using the nuisance parameter technique. The offsets show how the mean value of the measured cross section is shifted due to each source of systematic uncertainty. In each line, all but the considered source of systematic uncertainty are ignored. The $\pm\sigma$ give the impact on the measured cross section when the nuisance parameters describing the considered category are changed by ± 1 SD of their fitted value. See text for further details.

Source	$\ell\ell$				$\ell\ell+\ell j$			
	$\sigma_{t\bar{t}}$ [pb]	Offset [pb]	$+\sigma$ [pb]	$-\sigma$ [pb]	$\sigma_{t\bar{t}}$ [pb]	Offset [pb]	$+\sigma$ [pb]	$-\sigma$ [pb]
Statistical only		+8.04	+0.50	-0.48	+7.72		+0.20	-0.20
Muon identification		+0.00	+0.13	-0.12		-0.06	+0.06	-0.06
Electron identification and smearing		-0.22	+0.28	-0.25		+0.05	+0.13	-0.13
Signal modeling		+0.05	+0.39	-0.34		-0.04	+0.17	-0.15
Triggers		-0.01	+0.07	-0.07		-0.10	+0.10	-0.10
Jet energy scale		-0.16	+0.16	-0.15		-0.01	+0.03	-0.03
Jet reconstruction and identification		-0.21	+0.24	-0.22		+0.24	+0.08	-0.08
b-tagging		+0.14	+0.00	+0.00		-0.04	+0.16	-0.12
Background normalization		-0.27	+0.27	-0.25		-0.07	+0.11	-0.11
Instrumental background		-0.08	+0.19	-0.19		-0.01	+0.05	-0.05
Luminosity		-0.66	+0.59	-0.51		-0.43	+0.45	-0.40
Other		-0.04	+0.12	-0.11		-0.50	+0.58	+0.52
Template statistics		+0.00	+0.09	+0.09		+0.00	0.04	-0.04
Total systematics		-1.46	+0.89	+0.80		-0.50	+0.58	+0.52
Fit result	7.42		+0.90	-0.79	7.61		+0.63	-0.57

uncertainties for this combined measurement are summarized in Table II.

Due to acceptance effects, the $t\bar{t}$ efficiency depends on the assumed top quark mass in the MC. We extract the $t\bar{t}$ cross sections using the selection described above assuming different values of m_t using fully simulated $t\bar{t}$ events. The resulting cross sections can be fitted with the following functional form:

$$\sigma_{t\bar{t}}(m_t) = \frac{1}{m_t^4} [a + b(m_t - 170) + c(m_t - 170)^2 + d(m_t - 170)^3] \quad (5)$$

with $a = 6.57141 \times 10^9$, $b = 7.96467 \times 10^7$, $c = 9.30737 \times 10^5$ and $d = -2.770 \times 10^3$ and where $\sigma_{t\bar{t}}$ and m_t are in pb and GeV respectively. Figure 2 shows this parameterization for the measurement as a function of top quark mass together with approximate NNLO computations [1–3].

V. CONCLUSION

In this letter we presented an updated measurement of the $t\bar{t}$ production cross section in the dilepton final state using 5.4 fb⁻¹ of data. This cross section measurement yields $7.4_{-0.8}^{+0.9}$ (stat + syst) pb and has a relative precision of $_{-11\%}^{+12\%}$. It is currently the most precise measurement of the $t\bar{t}$ cross section in the dilepton channel. Combining the measurement in the dilepton channel with the result in the lepton + jets channel [6] yields 7.6 ± 0.6 (stat + syst) pb which corresponds to a relative precision of 8%. This measurement is in good agreement with the SM prediction.

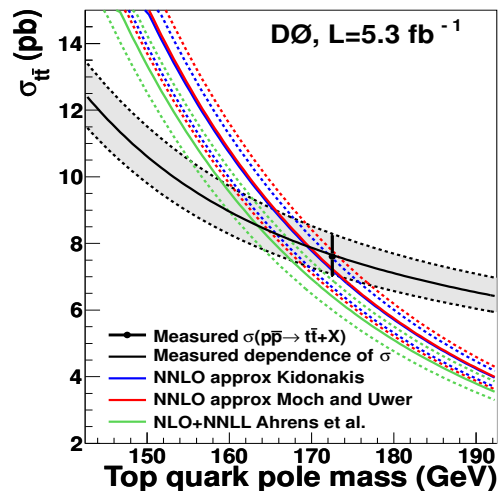


FIG. 2: Dependence of the experimental and theoretical [1–3] $t\bar{t}$ cross sections with the top quark mass. The point shows the combined $\ell\ell$ and ℓj cross section measurement for $m_t = 172.5$ GeV.

We thank the staffs at Fermilab and collaborating institutions, and acknowledge support from the DOE and NSF (USA); CEA and CNRS/IN2P3 (France); FASI, Rosatom and RFBR (Russia); CNPq, FAPERJ, FAPESP and FUNDUNESP (Brazil); DAE and DST (India); Colciencias (Colombia); CONACyT (Mexico); KRF and KOSEF (Korea); CONICET and UBACyT (Argentina); FOM (The Netherlands); STFC and the Royal

575 Society (United Kingdom); MSMT and GACR (Czech577
576 Republic); CRC Program and NSERC (Canada); BMBF578
and DFG (Germany); SFI (Ireland); The Swedish Re-
search Council (Sweden); and CAS and CNSF (China).

-
- 579 [1] V. Ahrens, A. Ferroglia, M. Neubert, B. D. Pecjak, and609
580 L. L. Yang, *J. High Energy Phys.* **1009**, 097 (2010);610
581 V. Ahrens, A. Ferroglia, M. Neubert, B. D. Pecjak, and611
582 L. L. Yang, *Nucl. Phys. Proc. Suppl.* **205–206**, 48 (2010).612
583 [2] S. Moch and P. Uwer, *PRD* **78**, 034003 (2008); U. Lan-613
584 genfeld, S. Moch, and P. Uwer, *PRD* **80**, 054009 (2009).614
585 [3] N. Kidonakis and R. Vogt, *PRD* **68**, 114014 (2003);615
586 N. Kidonakis, *PRD* **82**, 114030 (2010).616
587 [4] V. M. Abazov *et al.* (D0 Collaboration), *Phys. Lett. B*617
588 **679**, 177 (2009).618
589 [5] V. M. Abazov *et al.* (D0 Collaboration), *Phys. Rev. D*619
590 **80**, 071102 (2009).620
591 [6] V. M. Abazov *et al.* (D0 Collaboration), arXiv:1101.0124.621
592 [7] V. M. Abazov *et al.* (D0 Collaboration), *Phys. Rev. Lett.*622
593 **100**, 192004 (2008).623
594 [8] V. M. Abazov *et al.* (D0 Collaboration), *Phys. Rev. D* **76**,624
595 072007 (2007); V. M. Abazov *et al.* (D0 Collaboration),625
596 *Phys. Rev. D* **82**, 032002 (2010).626
597 [9] V. M. Abazov *et al.* (D0 Collaboration), *Phys. Lett. B*627
598 **626**, 55 (2005).628
599 [10] T. Aaltonen *et al.* (CDF Collaboration), *Phys. Rev. D*629
600 **82**, 052002 (2010).630
601 [11] G. Aad *et al.* (ATLAS Collaboration), arXiv:1012.1792.631
602 [12] V. Khachatryan *et al.* (CMS Collaboration),632
603 *Phys. Lett. B* **695**, 424 (2011).633
604 [13] V. M. Abazov *et al.* (D0 Collaboration), *Nucl. In-*634
605 *strum. Methods Phys. Res. A* **565**, 463 (2006).635
606 [14] T. Andeen *et al.*, FERMILAB-TM-2365 (2007).636
607 [15] G. C. Blazey *et al.*, in *Proceedings of the Workshop*:637
608 “QCD and Weak Boson Physics in Run II,” edited by
U. Baur, R. K. Ellis, and D. Zeppenfeld (Fermilab,
Batavia, IL, 2000) p. 47; see Sec. 3.5 for details.
[16] V. M. Abazov *et al.* (D0 Collaboration) *Nucl. In-*
strum. Methods Phys. Res. A **620**, 490 (2010).
[17] V. M. Abazov *et al.* (D0 Collaboration), *Phys. Rev. D*
76, 052006 (2007).
[18] M. L. Mangano, M. Moretti, F. Piccinini, R. Pittau, and
A. D. Polosa, *J. High Energy Phys.* **0307**, 001 (2003).
[19] T. Sjostrand, S. Mrenna, and P. Z. Skands, *J. High En-*
ergy Phys. **0605**, 026 (2006).
[20] J. Pumplin *et al.*, (CTEQ Collaboration), *J. High Energy*
Phys. **07**, 012 (2002).
[21] R. Gavin, Y. Li, F. Petriello and S. Quackenbush,
arXiv:1011.3540 [hep-ph].
[22] R. K. Ellis, *Nucl. Phys. Proc. Suppl.* **160**, 170 (2006).
[23] S. Frixione and B. R. Webber, arXiv:hep-ph/0612272.
[24] A. Buckley, H. Hoeth, H. Lacker, H. Schulz and J. E. von
Seggern, *Eur. Phys. J. C* **65**, 331 (2010);
P. Z. Skands and D. Wicke, *Eur. Phys. J. C* **52**, 133
(2007).
[25] P. M. Nadolsky *et al.*, *Phys. Rev. D* **78**, 013004 (2008).
[26] Y. Peters, K. Hamacher and D. Wicke, FERMILAB-TM-
2425-E.
[27] P. Sinervo, *In the Proceedings of PHYSTAT2003: Sta-*
tistical Problems in Particle Physics, Astrophysics, and
Cosmology, Menlo Park, California, 8-11 Sep 2003, pp
TUAT004.
[28] The pseudorapidity is defined as $\eta = -\ln[\tan(\theta/2)]$,
where θ is the polar angle with respect to the proton
beam.